MITSUBISHI ELECTRIC RESEARCH LABORATORIES
https://www.merl.com

# Flying Start of Sensorless Synchronous Machines with Reactive Power Injection

Anantaram, Varatharajan; Goldsmith, Abraham; Wang, Yebin

TR2023-037 May 16, 2023

**Abstract**

In this work, a flying start of sensorless synchronous machines based on the reactive power injection is proposed to identify the initial rotor position and angular speed under non-stationary conditions. This is realized with a novel control structure designed in the stator current reference frame such that it produces negligible braking torque and has minimal disturbances on the load. The proposed method benefits from a simple structure, low reliance on the motor model and is applicable to the family of synchronous machines. Moreover, the paper provides guidelines for gain selection based on the nominal nameplate parameters and discusses sensitivity analysis to errors in stator resistance. The proposed method is validated in simulation on a 5.5 kW permanent magnet-assisted synchronous reluctance (PM-SyR) machine.

*IEEE International Electric Machines and Drives Conference (IEMDC) 2023*



Mitsubishi Electric Research Laboratories, Inc.
201 Broadway, Cambridge, Massachusetts 02139

# Flying Start of Sensorless Synchronous Machines with Reactive Power Injection


Anantaram Varatharajan
*Mitsubishi Electric Research Labs*
Cambridge, MA 02139, USA
varatharajan@ieee.org

Abraham Goldsmith
*Mitsubishi Electric Research Labs*
Cambridge, MA 02139, USA
goldsmith@merl.com

Yebin Wang
*Mitsubishi Electric Research Labs*
Cambridge, MA 02139, USA
yebinwang@ieee.org



***Abstract*—In this work, a flying start of sensorless synchronous machines based on the reactive power injection is proposed to identify the initial rotor position and angular speed under non-stationary conditions. This is realized with a novel control structure designed in the stator current reference frame such that it produces negligible braking torque and has minimal disturbances on the load. The proposed method benefits from a simple structure, low reliance on the motor model and is applicable to the family of synchronous machines. Moreover, the paper provides guidelines for gain selection based on the nominal nameplate parameters and discusses sensitivity analysis to errors in stator resistance. The proposed method is validated in simulation on a 5.5 kW permanent magnet-assisted synchronous reluctance (PM-SyR) machine.**



***Index Terms*—Sensorless control, flying start, synchronous machines, reactive power injection, virtual resistance.**


## I. Introduction

The knowledge of initial rotor position is vital in the starting of the sensorless drives and engaging the closed-loop field-oriented-control. The sensorless drives commonly refers to the control of a motor without a position transducer. The literature is rich in different sensorless control techniques for low speeds based on magnetic saliency [1]–[3] and high speeds region based on the fundamental back-emf [4]–[6].

Some applications/instances have non-zero initial rotor speed (e.g. a brief power interruption to a high inertial drive). The flying start commonly refers to the estimation of initial mechanical states at non-stationary rotor conditions. Most established sensorless techniques are ill-suited for the flying start application, particularly at high speeds in permanent magnet synchronous machines (PMSM) due to the risk of back-emf inducing a large inrush current. The high frequency injection techniques exploiting the saliency are prevalent at low speeds but synchronous reluctance (SyR) machines have poor saliency at zero currents due to unsaturated ribs.

Among the methods that do not require an additional voltage sensor, a popular approach is the injection of a sequence of zero-voltage pulses [7]–[9] and evaluating the machine dynamic response; this relies on the motor parameters and subjects load to jerk-like disturbances. Alternatively, a virtual impedance based approach is proposed for non-salient PMSM in [10], [11] where the value of the virtual resistance is closed-loop adjusted for current regulation. However, the load is subjected to a continuous braking torque.

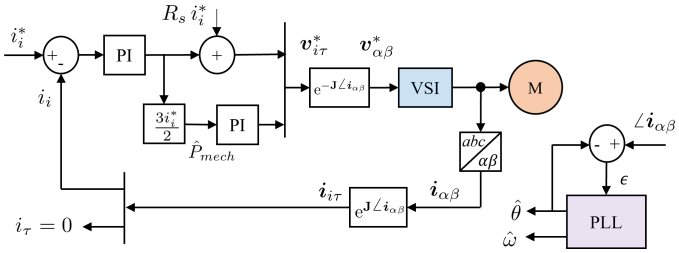


Fig. 1. Block diagram of the proposed flying start method with reactive power injection designed in the $i\tau$ stator current reference frame.

This paper presents a novel flying start method that has minimal load disturbances and is independent of motor parameters. This is achieved via reactive power injection and regulating the active power (and hence, the braking torque) to zero. The main contributions of this work are:

1) A reactive power injection based flying start method is proposed for the family of synchronous machines and is realized with a novel control structure in the stator current reference frame.
2) Unlike the state-of-art methods, the braking torque in the proposed scheme is zero, and hence, the impact on the load is minimal.
3) The position observer converges with zero steady-state error. Guidelines on tuning and gain selection based on nominal nameplate parameters are discussed.
4) The proposed technique is resilient to stator resistance variations. No other parameter is necessary.

The rest of the paper is organized as follows: Section II introduces the mathematical model and notations, and discusses the shortcomings of the state-of-art virtual resistance method. Section III presents the design and discussion on the proposed reactive power injection method. Section IV presents simulation results on a 5.5 PM-SyR machine and Section V concludes the paper.

## II. Flying Start Sensorless Control System

The electrical rotor position is $\theta$ and the electrical angular speed is $\omega = s\,\theta$ where $s$ is the differential operator $\frac{\mathrm{d}}{\mathrm{dt}}$. Estimated vectors are represented by the superscript $\hat{}$. The orthogonal rotational matrix is $\mathbf{J} = \left[\begin{smallmatrix} 0 & -1 \\ 1 & 0 \end{smallmatrix}\right]$ and $\mathbf{I}$ is the identity matrix.

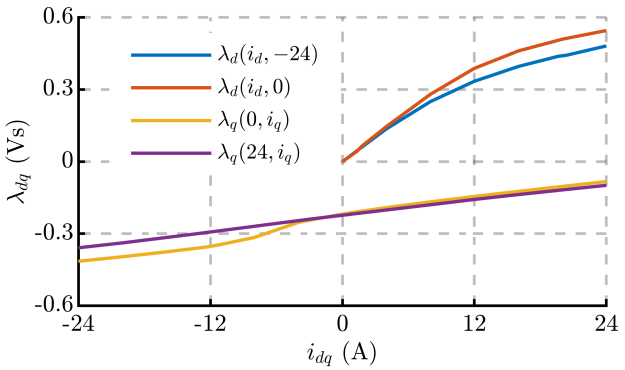


Fig. 2. Flux map of the 75.5 kW PM-SyR motor under test, experimentally identified with the constant speed test [12].

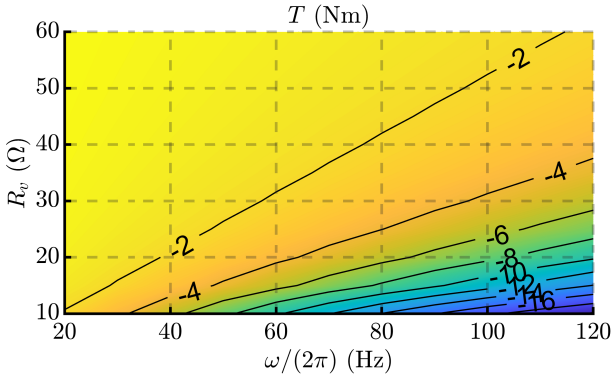


Fig. 3. Analytical evaluation of the steady-state braking torque for the virtual resistance flying start method; contours are plotted as functions of the rotor speed (0.2 - 2 p.u.) and the virtual resistance.

Real space vectors will be used; for example, the stator current is $\boldsymbol{i}_{dq} = [i_d, i_q]^{\mathrm{T}}$ where $i_d$ and $i_q$ are the vector components in rotor reference frame. Space vectors in the stationary reference frame are denoted by subscript $\alpha\beta$. Note that the convention of a SyR machine is followed, i.e, $d$-axis is defined along the maximum inductance path. Magnets, if any, are along the negative $q$-axis.

### A. Mathematical Model in dq Reference Frame

The voltage equation of a synchronous machine in rotor reference frame is expressed as

$$s\,\boldsymbol{\lambda}_{dq} = \boldsymbol{v}_{dq} - R_s \boldsymbol{i}_{dq} - \omega\,\mathbf{J}\,\boldsymbol{\lambda}_{dq} \tag{1}$$

where $R_s$ is the stator resistance and $\boldsymbol{\lambda}_{dq}$ is the stator flux linkage. The incremental inductance is defined as

$$\boldsymbol{L}_\partial = \frac{\partial \boldsymbol{\lambda}_{dq}}{\partial \boldsymbol{i}_{dq}} = \begin{bmatrix} l_d & l_{dq} \\ l_{dq} & l_q \end{bmatrix} \tag{2}$$

where $l_d, l_q$ represents the incremental inductance along direct $d$ and quadrature $q$-axis, respectively, while $l_{dq}$ is the cross-saturation term. All quantities are functions of $\boldsymbol{i}_{dq}$. The stator flux linkage is expressed as

$$\boldsymbol{\lambda}_{dq} = \boldsymbol{L}(\boldsymbol{i}_{dq}) \cdot \boldsymbol{i}_{dq} + \boldsymbol{\lambda}_m = \begin{bmatrix} L_d & 0 \\ 0 & L_q \end{bmatrix} \cdot \boldsymbol{i}_{dq} + \begin{bmatrix} 0 \\ -\lambda_m \end{bmatrix} \tag{3}$$

where $\boldsymbol{L}$ is the apparent inductance matrix and $\lambda_m$ is the open circuit permanent magnet flux linkage; $\lambda_m = 0$ corresponds to the SyR machine. The saturation and cross-saturation properities of the PM-SyR machine under test is illustrated in the flux-map in Fig. 2 that is experimentally identified with constant speed test reported in [12].

The average electromagnetic torque of a synchronous machine is given by

$$T = \frac{3p}{2}\, \boldsymbol{i}_{dq}^{\mathrm{T}}\, \mathbf{J}\, \boldsymbol{\lambda}_{dq} \tag{4}$$

where $p$ is the number of pole pairs.

### B. Flying Start with Virtual Resistance Method

The virtual resistance based flying start [10] is among the state-of-art method to estimate the initial mechanical states. The inverter output voltage and the maximum virtual resistance condition are given by

$$\boldsymbol{v}_{\alpha\beta} = -R_v\, \boldsymbol{i}_{\alpha\beta} \qquad 0 < R_s + R_v < \frac{L_q}{T_s} \tag{5}$$

where $R_v$ is the virtual resistance and $T_s$ is the sampling time. For the voltage (5), the dynamics of the stator current derived from (1) and (3) are governed by

$$\boldsymbol{i}_{dq} = \frac{-\omega\,\mathbf{J}\,\boldsymbol{\lambda}_m}{(R_v + R_s)\,\mathbf{I} + \omega\,\mathbf{J}\,\boldsymbol{L} + s\,\boldsymbol{L}_\partial} \tag{6}$$

and the $dq$ steady-state currents are given by

$$\boldsymbol{i}_{dq} = -\omega \left( (R_v + R_s)\,\mathbf{I} + \omega\,\mathbf{J}\,\boldsymbol{L} \right)^{-1} \mathbf{J}\,\boldsymbol{\lambda}_m. \tag{7}$$

Using (7) in (4), the resulting steady-state braking torque is computed and shown in Fig. 3 as functions of the angular rotor speed and the virtual resistance for the machine under test. The braking torque is observed to increase with increasing rotor speed and decreasing virtual resistance; it is, however, always non-zero and the machine is susceptible to disturbances. Having $R_v = -R_s$ in (7) results in zero torque ($i_d = 0$) but the poles in (6) become purely imaginary that is practically unstable.

The rotor position estimation uses a phase-locked-loop (PLL) to track the stator current, i.e,

$$\hat{\theta} = \angle \boldsymbol{i}_{\alpha\beta} \tag{8}$$

where $\hat{\theta}$ is the estimated rotor position. The stator current (7) converges to the second quadrant for positive motor speed (and first quadrant for negative motor speed), leading to a steady-state position error given by $\tilde{\theta} = \theta - \hat{\theta} = \angle \boldsymbol{i}_{dq}$. Fig. 4 shows the position error contour where it is observed to increases with the virtual resistance. Thus, additional compensation that is equal to the current angle (7) based on the machine parameters is necessary for the position error correction.

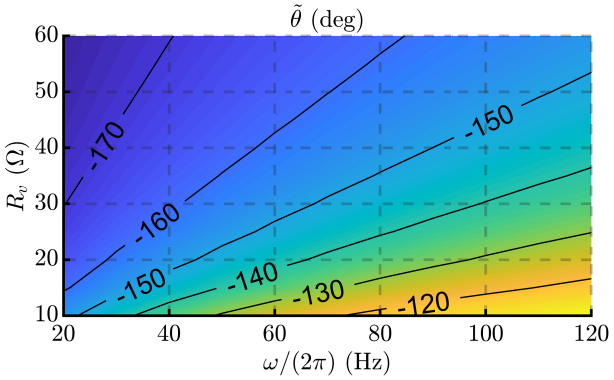


Fig. 4. Analytical evaluation of the position error for the virtual resistance flying start method; contours are plotted as functions of the rotor speed (0.2 - 2 p.u.) and the virtual resistance.

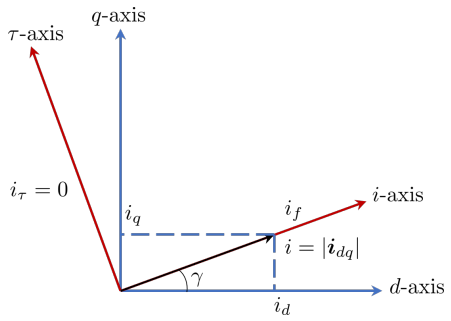


Fig. 5. Illustration of the $i\tau$ reference frame where the $i$-axis is oriented along the stator current vector.

Alternatively, a virtual impedance has been proposed [11] with resistive ($R_v$) and inductive ($L_v$) components as

$$\boldsymbol{v}_{\alpha\beta} = -(R_v + sL_v)\,\boldsymbol{i}_{\alpha\beta} \tag{9}$$

where the steady-state stator current expression becomes

$$\boldsymbol{i}_{dq} = -\omega\left((R_v + R_s)\,\mathbf{I} + \omega\,\mathbf{J}\,(\boldsymbol{L} + L_v\mathbf{I})\right)^{-1}\mathbf{J}\,\boldsymbol{\lambda}_m. \tag{10}$$

Using $L_v\mathbf{I} = \boldsymbol{L}$ mitigates the position error and the stator current converges to the $d$-axis ($i_q = 0$). However, this is only valid for non-salient surface PMSM machines ($L_d = L_q$). Moreover, the braking torque due to the magnetic component is non-zero.

## III. Proposed Reactive Power Injection Method

The block diagram of the proposed flying start method is shown in Fig. 1 and is implemented in the $i\tau$ stator current reference frame.

### A. Mathematical Model in $i\tau$ Reference Frame

The stator current reference frame, shown in Fig. 5, is denoted by the subscript $i\tau$ where the $i$-axis is aligned along the stator current vector and $\tau$-axis is the quadrature axis, i.e.,

$$\boldsymbol{i}_{i\tau} = \begin{bmatrix} i_i \\ 0 \end{bmatrix} = \mathrm{e}^{-\mathbf{J}\gamma}\cdot\boldsymbol{i}_{dq} \tag{11}$$

where $i_i = |\boldsymbol{i}_{dq}|$ is the current magnitude and $\gamma = \angle\boldsymbol{i}_{dq}$ is the current angle. The voltage equation (1) transforms to

$$\mathrm{e}^{\mathbf{J}\gamma}\boldsymbol{L}_\partial\,\mathrm{e}^{-\mathbf{J}\gamma}\begin{bmatrix} s\,i_i \\ i_i\,s\,\gamma \end{bmatrix} = \boldsymbol{v}_{i\tau} - R_s\begin{bmatrix} i_i \\ 0 \end{bmatrix} - \omega\,\mathbf{J}\,\boldsymbol{\lambda}_{i\tau} \tag{12}$$

where the state variables are $i_i$ and $\gamma$. The torque equation (4) simplifies to

$$T = \frac{3p}{2}\,\lambda_\tau\,i_i. \tag{13}$$

Thus, it follows that the voltage equation (12) can be rewritten in terms of active and reactive power as

$$\mathrm{e}^{\mathbf{J}\gamma}\boldsymbol{L}_\partial\,\mathrm{e}^{-\mathbf{J}\gamma}\begin{bmatrix} s\,i_i \\ i_i\,s\,\gamma \end{bmatrix} = \boldsymbol{v}_{i\tau} - R_s\begin{bmatrix} i_i \\ 0 \end{bmatrix} - \frac{2}{3\,i_i}\begin{bmatrix} P_{mech} \\ Q \end{bmatrix} \tag{14}$$

where $Q$ is the reactive power and $P_{mech}$ is the mechanical active power output. For simplicity in analysis, the cross-saturation inductance is neglected, $l_{dq} = 0$, i.e.,

$$\mathrm{e}^{\mathbf{J}\gamma}\boldsymbol{L}_\partial\,\mathrm{e}^{-\mathbf{J}\gamma} = \begin{bmatrix} l_\Sigma + l_\Delta\,\cos(2\gamma) & l_\Delta\,\sin(2\gamma) \\ l_\Delta\,\sin(2\gamma) & l_\Sigma - l_\Delta\,\cos(2\gamma) \end{bmatrix} \tag{15}$$

where $l_\Sigma = (l_d + l_q)/2$ and $l_\Delta = (l_d - l_q)/2$.

### B. Control System for Reactive Power Injection

The proposed control scheme has two objectives: *(i)* inject a constant stator current of magnitude $i_i^*$ and *(ii)* ensure the active power is driven to zero, $P_{mech} = 0$, to mitigate the braking torque disturbances. To this end, a proportional-integral (PI) controller in the $i$-axis is designed to establish a constant current $i_i = i_i^*$ as

$$v_i^* = \left(k_{pi} + \frac{k_{ii}}{s}\right)(i_i^* - i_i) + R_s\,i_i \tag{16}$$

where $k_{pi}$ and $k_{ii}$ are the proportional and integral gains, respectively. An orthogonal $\tau$-axis controller is used to regulate the active power to zero, $P_{mech}$. Assuming $i_i^* \approx i_i$, the active power estimate $\hat{P}_{mech}$ can be expressed as

$$\hat{P}_{mech} = \frac{3\,i_i}{2}\left(v_i^* - R_s\,i_i\right) \tag{17}$$

Thus, the $\tau$-axis PI controller is designed as the following:

$$v_\tau^* = \left(k_{p\tau} + \frac{k_{i\tau}}{s}\right)\hat{P}_{mech} \tag{18}$$

where and $k_{p\tau}$ and $k_{i\tau}$ are the corresponding gains.

### C. Tuning Guidelines

The controller gains are tuned by representing the control variables ($i_i$ and $P_{mech}$) in terms of the state variables ($i_i$ and $\gamma$). The $i$-axis gains for the critically damped poles at $s = -\Omega_i$ are given by

$$k_{pi} = \mu_i\,2\,\Omega_i \qquad k_{ii} = \mu_i\,\Omega_i^2 \tag{19}$$

where the scaling factor $\mu_i$ follows from (14) and (15) as

$$\mu_i = l_\Sigma + l_\Delta\,\cos(2\gamma). \tag{20}$$

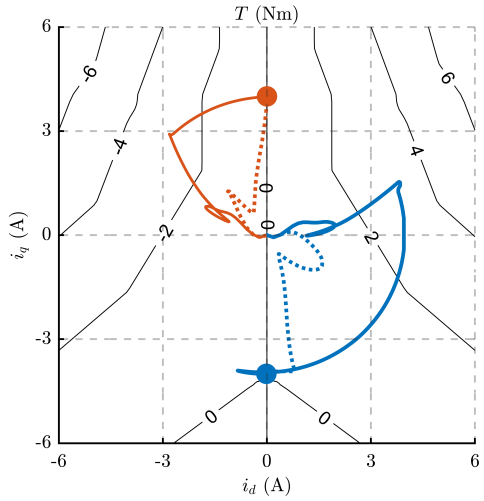


Fig. 6. Simulated current trajectories of the proposed technique shown against the torque contour in black. Positive rated speed $\omega = 2\pi \cdot 60$ rad/s (1800 rpm) is shown in red and negative rated speed $\omega = -2\pi \cdot 60$ rad/s(-1800 rpm) in blue. The solid lines have slow $\tau$-axis dynamics $\Omega_\tau = 2\pi \cdot 10$ rad/s and the dotted lines have faster dynamics $\Omega_\tau = 2\pi \cdot 50$ rad/s. Marker $\circ$ denotes the steady-state settling point. The current reference is $i_i^* = 4$ A, satisfies (24).

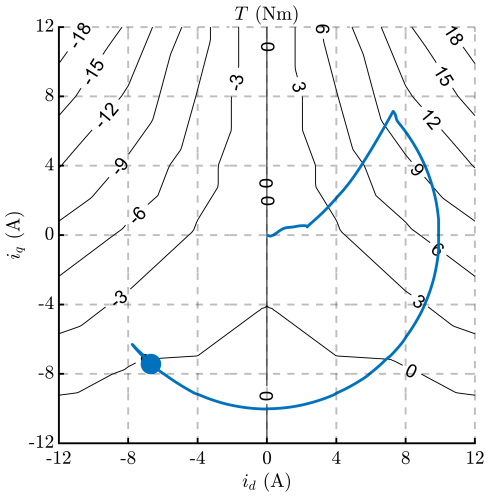


Fig. 7. Simulated current trajectories of the proposed technique at negative rated speed $\omega = -2\pi \cdot 60$ rad/s(-1800 rpm) and $\Omega_\tau = 2\pi \cdot 10$ rad/s. Marker $\circ$ denotes the steady-state settling point. The current reference is $i_i^* = 10$ A, violates (24) leading to position estimation error.

Likewise, the $\tau$-axis gains are tuned for critically damped poles at $s = -\Omega_\tau$ as

$$k_{p\tau} = \mu_\tau \, 2\,\Omega_\tau \qquad k_{i\tau} = \mu_\tau \, \Omega_\tau^2. \tag{21}$$

The scaling factor $\mu_\tau$ is computed from the linearized model as

$$\mu_\tau = \frac{i\left(l_\Sigma - l_\Delta \, \cos(2\gamma)\right)}{\partial P_{mech}/\partial\gamma} \tag{22}$$

where the term $\partial P_{mech}/\partial\gamma$ can be expressed as

$$\frac{\partial P_{mech}}{\partial\gamma} = \frac{3}{2}\,\omega\left(l_\Delta \, i^2 \, 2\cos(2\gamma) - \lambda_m \, i \, \sin(\gamma)\right) \tag{23}$$

It is apparent that the scaling factors are operating point dependent. Hence, an approximate gains are computed using the nominal parameters at rated speed and considering the initial condition $\gamma = 0$.

### D. Convergence Discussion

For positive angular speeds, the open-circuit back-emf due to the magnets in the negative $q$-axis is directed along the negative $d$-axis. Hence, the initial $dq$ stator current evolves in the braking region in second/third quadrant. The negative mechanical active power ($P_{mech}$) is input to the $\tau$-axis controller that drives the state variable $\gamma$ in the clockwise direction. This leads to the convergence of the stator currents to the zero-torque locus in the positive $q$-axis.

Fig. 6 illustrates the evolution of the $dq$ current trajectories juxtaposed against the torque contour. The results for the flying start at positive rated speed (shown in red) appear in the negative torque region and converge to the positive $q$-axis. The solid curves correspond to the test with slow $\tau$-axis dynamics to help illustrate the convergence where the stator current is observed to move along the constant current locus, $i_i^* = i_i = 4$ A, towards the $q$-axis.

Similar discussion follows for the flying start at negative angular speed where the currents evolve in the positive torque region in first/fourth quadrant. However, to ensure that the stator currents settle in the zero-torque locus in the negative $q$-axis, the maximum $i_i$ should be limited to

$$i_i < \frac{\lambda_m}{L_q}. \tag{24}$$

Fig. 6 is set to the maximum value $i_i = 4$ A. For higher values of $i_i$, the negative $q$-axis is no longer a stable equilibrium and the control settles on the zero-torque locus in the third quadrant as shown in Fig. 7, leading to inaccurate initial position estimation. No such limitation on $i_i$ exist for synchronous reluctance machines without magnets.

### E. Position Observer

A conventional phase-locked-loop (PLL) with a proportional-integral (PI) controller is employed to drive the error signal $\epsilon$ to zero as in (25)

$$\hat{\omega} = k_p\,\epsilon + \int k_i\,\epsilon\,\mathrm{d}t \qquad \hat{\theta} = \int \hat{\omega}\,\mathrm{d}t \tag{25}$$

where $k_p$ and $k_i$ are the respective gains; the gains are tuned for critically damped poles at $s = -\Omega_\omega$. The position error signal to track the stator current is given by

$$\epsilon = \angle \boldsymbol{i}_{\alpha\beta} - \hat{\theta} \tag{26}$$

where $\hat{\theta}$ is the estimated position. Note that the PLL converges to the $q$-axis and a correction of $\pm\pi/2$ based on the direction of angular speed is necessary to orient along the $d$-axis.

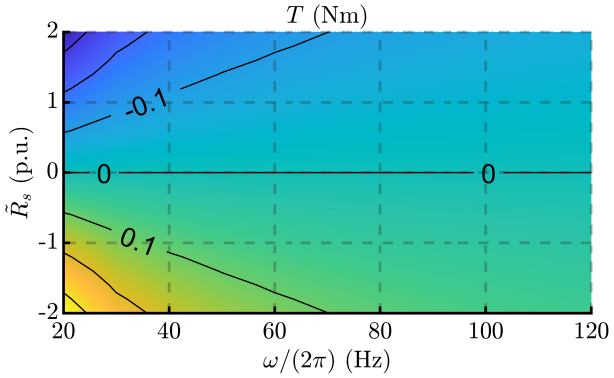


Fig. 8. Sensitivity analysis to stator resistance: contour of the steady-state torque plotted as functions of the rotor speed (0.2 - 2 p.u.) and the resistance error ($\tilde{R}_s = \pm 2$ p.u. $\Rightarrow \hat{R}_s = \pm 3\, R_s$).

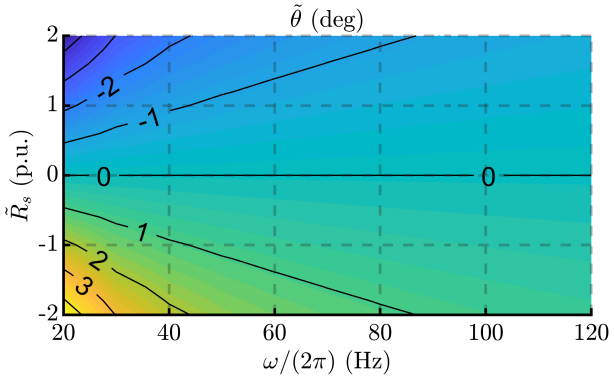


Fig. 9. Sensitivity analysis to stator resistance: contour of the steady-state position error plotted as functions of the positive rotor speed and the resistance error ($\tilde{R}_s = \pm 2$ p.u. $\Rightarrow \hat{R}_s = \pm 3\, R_s$).

### F. Sensitivity to Stator Resistance

Let $\tilde{R}_s = R_s - \hat{R}_s$ denote the resistance error where $\hat{R}_s$ is the estimated resistance. Then, it follows from (1) and (17) that in steady-state,

$$\frac{3\, i_i}{2}\left(v_i^* - \hat{R}_s\, i_i\right) = 0 \qquad \Rightarrow \qquad \lambda_\tau = -\frac{\tilde{R}_s\, i_i}{\omega}. \tag{27}$$

Thus, the residual torque and active power are given by

$$T = -\frac{3p}{2}\,\frac{\tilde{R}_s\, i_i^2}{\omega} \qquad \Rightarrow \qquad P_{mech} = -\frac{3}{2}\,\tilde{R}_s\, i_i^2 \tag{28}$$

The contour of the torque (28) as functions of rotor speed and resistance error is shown in Fig. 8 and is observed to insignificant, particularly at medium/high speeds. The steady-state position error for positive and negative speeds under resistance error is shown in Figs. 9 and 10, respectively. The negative low speeds region is more sensitive, yet the position error is $|\tilde{\theta}| < 10^\circ$ for resistance error $|\tilde{R}_s| < 1$ p.u. ($|\hat{R}_s| < 2\, R_s$).

## IV. Simulation

The proposed flying start method is validated in the Matlab Simulink environment. The parameter of the PM-SyR machine

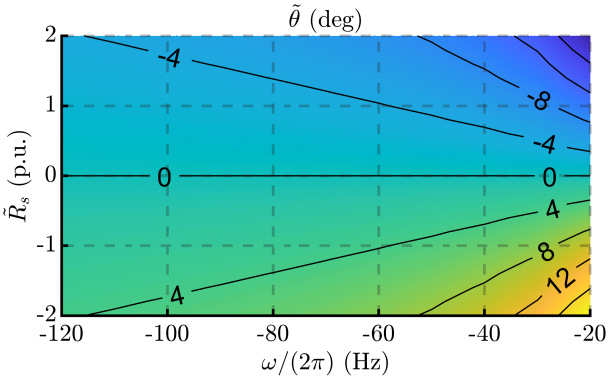


Fig. 10. Sensitivity analysis to stator resistance: contour of the steady-state position error plotted as functions of the negative rotor speed and the resistance error ($\tilde{R}_s = \pm 2$ p.u. $\Rightarrow \hat{R}_s = \pm 3\, R_s$).

TABLE I
PM-SyR Motor Parameters

| Parameters | Symbol | Values | Units |
|---|---|---|---|
| Rated power | $P_n$ | 5.52 | kW |
| Rated voltage (line rms) | $V_n$ | 260 | V |
| Rated speed | $\omega_n$ | 1800 | rpm |
| Rated current (rms) | $I_n$ | 16.3 | A |
| Rated torque | $T_n$ | 29.8 | Nm |
| Pole pairs | $p$ | 2 | - |
| Stator resistance | $R_s$ | 0.46 | Ω |
| PM flux magnitude | $\lambda_m$ | 0.22 | Vs |
| $d$-axis inductance | $L_d$ | 24 | mH |
| $q$-axis inductance | $L_q$ | 7 | mH |

under test is tabulated in Table. I. The flying start operation is considered at no-load with a shaft inertia $J = 0.02$ kg m$^2$. The switching frequency of the system is 10 kHz.

The PLL poles are placed at $\Omega_\omega = 2\pi \cdot 60$ rad/s. The $i$-axis current controller is tuned for $\Omega_i = 2\pi \cdot 150$ rad/s and $\tau$-axis controlled for $\Omega_\tau = 2\pi \cdot 50$ rad/s.

### A. Virtual Resistance Based Flying Start

The performance of the virtual resistance based flying start method at rated speed $\omega = 1800$ rpm (60 Hz electrical) is shown in Fig. 11 where the drive is powered-up at time $t = 0$ s. A constant virtual resistance $R_v = -20\,\Omega$ is considered. For $t > 0$ s, the braking torque is $T = -3.5$ Nm and the steady-state position error $\tilde{\theta} = -145^\circ$, in agreement with Figs. 4 and 3, respectively. The rotor speed (magnified shown in red dotted line) decelerates by 160 rpm in 100 ms for the considered shaft inertia of $J = 0.02$ kg m$^2$.

### B. Reactive Power Injection Flying Start

The proposed flying start method using reactive power injection at positive and negative rated speed is shown in Figs. 12 and 13, respectively. The current reference with a ramp profile is set to the maximum limit satisfying (24), $i_i^* = 4$ A. Unlike the former, once the drive is powered-up at $t = 0$ s, barring a small transient, the braking torque remains negligible and the position error converges to zero. It is worth pointing

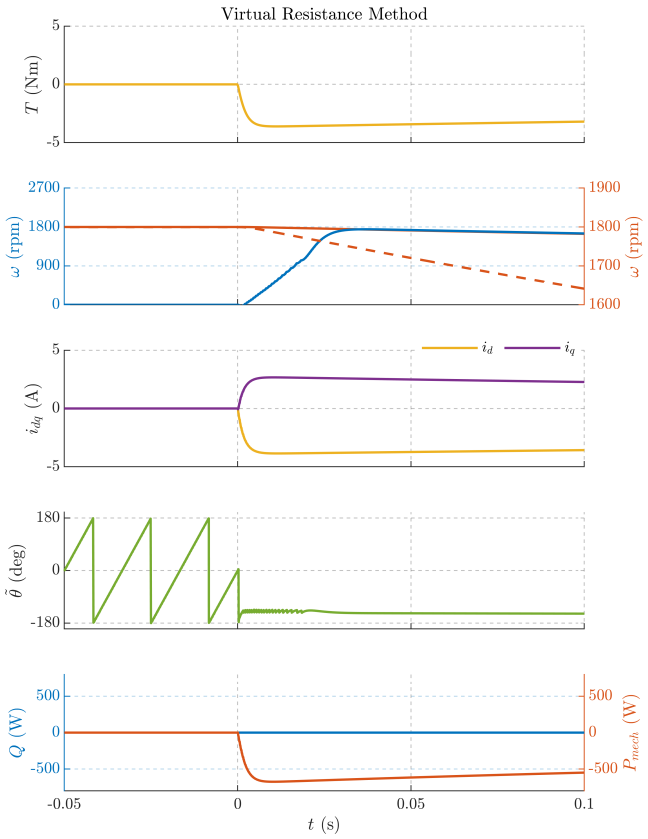


Fig. 11. Analysis of the virtual resistance based flying start method [10] when the drive is powered-up at time $t = 0$ s at the rated rotor speed $\omega = 1800$ rpm and no-load

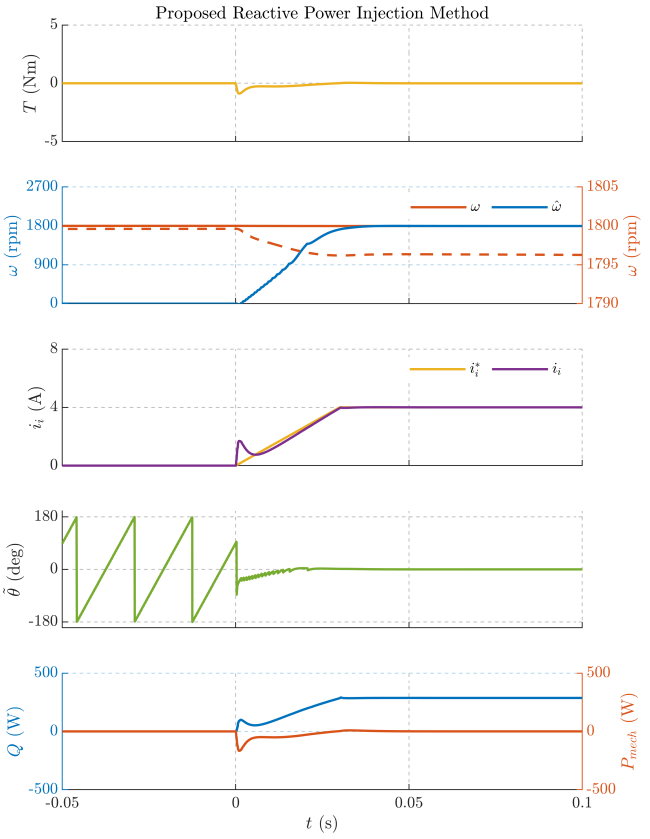


Fig. 12. Analysis of the proposed reactive power injection based flying start method when the drive is powered-up at time $t = 0$ s at the rated rotor speed $\omega = 1800$ rpm and no-load.

out that the rotor remains largely unperturbed and the speed nearly constant (speed reduction $< 5$ rpm).

### C. Validation of Resistance Sensitivity Analysis

The resistance sensitivity is validated at negative low speed region $\omega = -2\pi \cdot 20$ rad/s (0.33 p.u.) for a resistance error of $\hat{R}_s = 2\,R_s$ ($\tilde{R}_s = -1$ p.u.) as shown in Fig. 14. A steady-state torque $T = -0.2$ Nm and position error $\tilde{\theta} = 10°$ is observed, in agreement with the analytical evaluations in Figs. 8 and 10, respectively. Despite a high resistance error, the proposed method is sufficiently resilient.

## V. Conclusion

This paper proposed a novel flying start method for sensorless synchronous drives to estimate the initial rotor position and speed with least disturbances on the load. This is achieved by reactive power injection and realized in the stator current reference frame such that the operating point settles on the zero-torque locus. As opposed to the virtual resistance method, the rotor experiences minimal braking torque and the position error converges to zero in steady-state. Guidelines for tuning and gain selection based on the nominal parameters were discussed. Moreover, the proposed method benefits from a simple structure, resilience to resistance errors and less dependency on the motor parameters.

## References


[1] J. Lee, Y.-C. Kwon, and S.-K. Sul, "Signal-injection sensorless control with tilted current reference for heavily-saturated ipmsms," *IEEE Transactions on Power Electronics*, vol. 8993, pp. 1–1, 2020.

[2] V. Manzolini and S. Bolognani, "On the rotor position self-sensing capability of reluctance and ipm synchronous motors," *IEEE Transactions on Industry Applications*, vol. 56, pp. 3755–3766, 2020.

[3] A. Varatharajan, G. Pellegrino, and E. Armando, "Signal-injection sensorless control of synchronous reluctance machines for overload operation," *IEEE Transactions on Power Electronics*, vol. 37, pp. 5874–5883, 2022.

[4] S. C. Agarlita, I. Boldea, and F. Blaabjerg, "High-frequency-injection-assisted 'active-flux'-based sensorless vector control of reluctance synchronous motors, with experiments from zero speed," *IEEE Transactions on Industry Applications*, vol. 48, pp. 1931–1939, 2012.

[5] M. Hinkkanen, S. E. Saarakkala, H. A. A. Awan, E. Mölsä, and T. Tuovinen, "Observers for sensorless synchronous motor drives: Framework for design and analysis," *IEEE Transactions on Industry Applications*, vol. 54, pp. 6090–6100, 2018.

[6] A. Varatharajan, G. Pellegrino, E. Armando, and M. Hinkkanen, "Sensorless synchronous motor drives: A review of flux observer-based position estimation schemes using the projection vector framework," *IEEE Transactions on Power Electronics*, vol. 36, pp. 8171–8180, 2021.

[7] K. Lee, S. Ahmed, and S. M. Lukic, "Universal restart strategy for high-inertia scalar-controlled pmsm drives," *IEEE Transactions on Industry Applications*, vol. 52, no. 5, pp. 4001–4009, 2016.

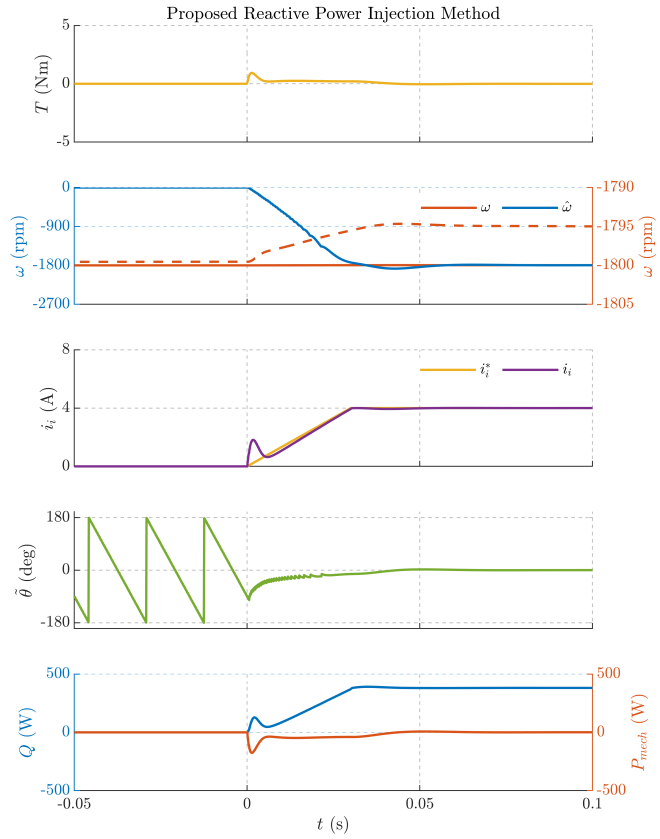


Fig. 13. Analysis of the proposed reactive power injection based flying start method when the drive is powered-up at time $t = 0$ s at the rated rotor speed $\omega = 1800$ rpm and no-load.

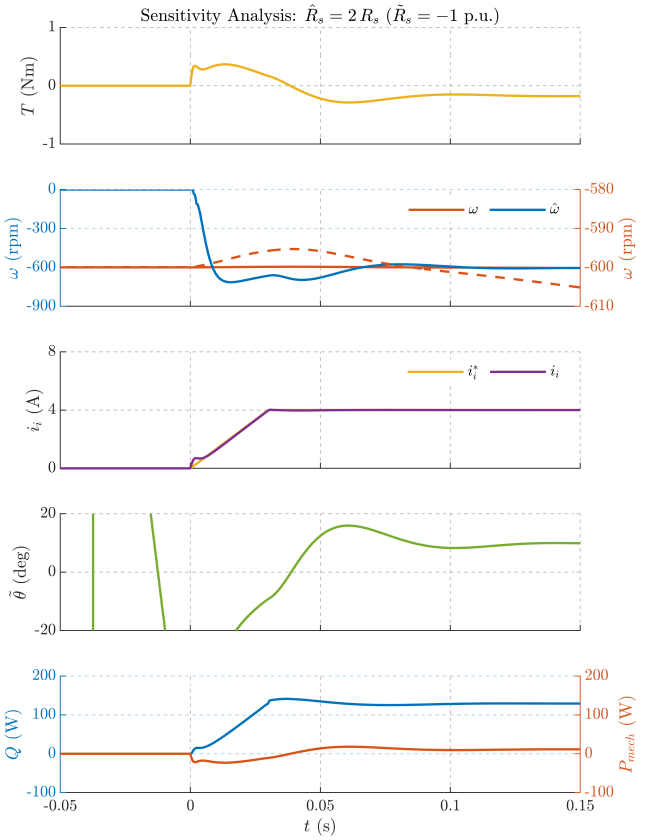


Fig. 14. Analysis of the proposed reactive power injection based flying start method when the drive is powered-up at time $t = 0$ s at the rated rotor speed $\omega = 1800$ rpm and no-load.


[8] L. Pravica, D. Sumina, and T. Bariša, "Flying start of a permanent magnet wind power generator based on a discontinuous converter operation mode and a phase-locked loop," *IEEE Transactions on Industrial Electronics*, vol. 65, no. 2, pp. 1097–1106, 2018.

[9] S. Taniguchi, S. Mochiduki, T. Yamakawa, S. Wakao, K. Kondo, and T. Yoneyama, "Starting procedure of rotational sensorless pmsm in the rotating condition," *IEEE Transactions on Industry Applications*, vol. 45, no. 1, pp. 194–202, 2009.

[10] K. M. Choo and C. Y. Won, "Flying start of permanent-magnet-synchronous-machine drives based on a variable virtual resistance," *IEEE Transactions on Industrial Electronics*, vol. 68, pp. 9218–9228, 2021.

[11] Y. S. Lee, K. M. Choo, W. S. Jeong, C. H. Lee, J. Yi, and C. Y. Won, "A virtual impedance-based flying start considering transient characteristics for permanent magnet synchronous machine drive systems," *Energies*, vol. 16, 2 2023.

[12] E. Armando, R. I. Bojoi, P. Guglielmi, G. Pellegrino, and M. Pastorelli, "Experimental identification of the magnetic model of synchronous machines," *IEEE Transactions on Industry Applications*, vol. 49, pp. 2116–2125, 2013.